SLAC-PUB-9680
March 2003

THE PHYSICS AND APPLICATIONS OF HIGH BRIGHTNESS BEAMS: WORKING GROUP A SUMMARY ON HIGH BRIGHTNESS BEAM PRODUCTION*

J.F. SCHMERGE

Stanford Linear Accelerator Center
2575 Sand Hill Rd,
Menlo Park, CA 94025, USA
E-mail: Schmerge@slac.stanford.edu

Presented at the Joint ICFA Advanced Accelerator and Beam Dynamics Workshop:
The Physics and Applications of High Brightness Electron Beams,
7/1/2002 - 7/6/2002, Chia Laguna, Sardinia, Italy

*Work supported by Department of Energy contract DE-AC03-76SF00515

THE PHYSICS AND APPLICATIONS OF HIGH BRIGHTNESS BEAMS: WORKING GROUP A SUMMARY ON HIGH BRIGHTNESS BEAM PRODUCTION*

J.F. SCHMERGE

Stanford Linear Accelerator Center
2575 Sand Hill Rd,
Menlo Park, CA 94025, USA
E-mail: Schmerge@slac.stanford.edu

Working group A was devoted to high brightness beam production and characterization. The presentations and discussions could be categorized as cathode physics, new photoinjector designs, computational modeling of high brightness beams, and new experimental methods and results. Several novel injector and cathode designs were presented. However, a standard 1.5 cell rf photoinjector is still the most common source for high brightness beams. New experimental results and techniques were presented and thoroughly discussed. The brightest beam produced in a rf photoinjector published at the time of the workshop is approximately 2 10^{14} A/(m-rad)^2 at Sumitomo Heavy Industries in Japan with 1 nC of charge, a 9 ps FWHM long laser pulse and a normalized transverse emittance of 1.2 pm. The emittance was achieved by utilizing a temporally flat laser pulse which decreased the emittance by an estimated factor of 2 from the beam produced with a Gaussian pulse shape with an identical pulse length.

1. Introduction

Working group A was devoted to high brightness electron beam production. More than 25 people attended the group sessions during which 16 talks were presented. The balance of the time was spent in discussions on methods to create higher brightness beams and other related issues. The presentations and discussion topics could be categorized as follows; cathode physics, new photoinjector designs, computational modeling of high brightness beams, and new experimental methods and results.

In addition there were several talks during the plenary sessions related to high brightness beam production. In one of the plenary sessions P. Piot presented a summary talk on the status of current high brightness sources. Among the graphs he presented is Figure 1 which shows the beam brightness plotted as a function of injector frequency with the laboratory conducting the

experiment labeled for each point. Two points of specific interest are the Sumitomo Heavy Industries (SHI) [1] and the ELSA 2 [2] experiments which both achieved normalized transverse emittances of 1 pm with 1 nC of charge. The low emittance in the SHI experiment was achieved by utilizing a 10 ps FWHM temporally flat laser pulse which decreased the emittance by an estimated factor of two from the beam produced with a Gaussian pulse shape with an identical length. More details of this experiment are discussed in section 5.1. The ELSA 2 experiment used a laser with Gaussian pulse shape but with a comparatively long pulse length of 60 ps due to the low rf frequency of 144 MHz. Both experiments have achieved the nominal emittance requirement of 1 pm with 1 nC of charge desired by many proposed light sources such as SASE FELs [3] and energy recovery linac based sources [4]. These are believed to be the first sources meeting the desired emittance specification.

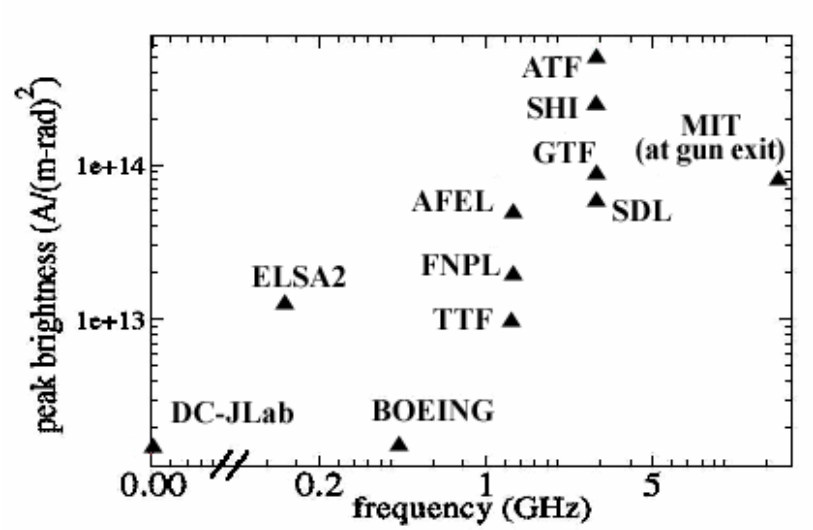

Figure 1. The plot shows peak beam brightness versus injector frequency. The brightest beams to date have been produced in S-band rf guns. The three brightest beams have all been produced with electrically identical 1.6 cell rf guns. The plot was provided by P. Piot.

Photoinjectors are currently the most common source used for high brightness beam production. One of the most popular designs is the BNL/SLAC/UCLA S-band gun with 1.6 cells. Electrically identical copies of this gun have been used to produce the three brightest beams plotted in Figure 1.

However, while 2856 MHz appears to be the most common frequency, there is no experimental evidence that it is the optimal frequency. In fact many of the novel injector designs are pushing to either very low frequency such as pulsed DC guns or extremely high frequency such as laser wakefield accelerator based injectors. It was the consensus of the group that the new technologies will require many years of development before they can exceed the performance from an rf photoinjector. However, it should be pointed out that after more than a decade of existence, rf photoinjectors are just now approaching the peak brightness predicted by simulations. Thus even though the new injector designs will require years of development, they can and should be pursued. Nonetheless it appears that the best available source for high brightness beams in the near future is likely to be a standard rf photoinjector.

Despite the abundance of rf photoinjectors, few have been able to meet the peak brightness predicted by simulation. The experimentalists in the group held the laser beam quality primarily responsible for the electron beam not achieving the optimal performance suggested by simulation. The best simulation results are always achieved by assuming an ideal electron beam. Thus the laser beam illuminating the cathode must have a flat-top profile in both the longitudinal and transverse dimensions in order to produce a uniform density cylinder of charge and achieve the peak brightness from a photoinjector. In addition the shot to shot fluctuations such as energy, position and timing need to be minimized in order to optimize the electron beam brightness.

While laser experts can easily produce one of the aforementioned laser qualities, it is much more difficult to produce all the desired qualities simultaneously with minimal jitter. It was the consensus of the group that to date the optimal rf photoinjector drive laser has yet to be designed and built. The desired laser is certainly not commercially available. Too often photoinjector based accelerators do not properly prioritize the drive laser system and consequently the appropriate cost and effort is not spent on the laser design and construction. The result is often accelerator physicists attempting to improve the performance of the drive laser in order to improve the electron beam quality.

Cathode emission uniformity also limits the experimentally achieved beam brightness. Most groups address this problem with so called laser cleaning where the laser fluence is increased to the point that surface contaminants can be vaporized. Surface contaminants produce local variations in the work function and thus once they are removed the cathode emission exhibits less spatial variation. This procedure needs to be repeated on a regular basis to maintain the quantum efficiency and uniformity. Of course the ideal method would be to

measure the electron distribution exiting the cathode and modify the laser spatial intensity to produce a uniform electron beam. While this idea has been around for many years it has yet to be experimentally implemented on an rf photoinjector. All the limiting factors described above must be addressed in order to achieve the peak available brightness from a standard rf photoinjector.

2. Cathode Physics

A physics limitations of beam brightness produced by a conventional rf photoinjector is the thermal emittance produced at the cathode. The total emittance exiting the injector is given approximately by the quadratic sum of the thermal emittance and the emittance produced in the injector due to time varying rf forces, space charge and other effects in the emittance compensation process. Measurement of the thermal emittance from a Cu cathode [5] resulted in an emittance of 0.6 μm per mm radius of the cathode which is approximately a factor of 2 larger than theoretical predictions. The total emittance in recent experiments have come close to the thermal emittance limit and therefore no substantial reductions in emittance can be achieved without reducing the thermal emittance. The group consensus was that the thermal emittance is rapidly becoming a beam brightness limiting factor. The emission process needs to be better understood to potentially reduce the thermal emittance. The penetration depth, laser polarization and surface roughness may all affect the thermal emittance. Unfortunately, to the author's knowledge, no experiments are in progress to directly measure the thermal emittance from photoinjector photo-cathodes.

A novel cathode type discussed at the workshop was needle cathodes. A needle cathode has a very small but sharp tip which greatly enhances the rf field and consequently concentrates the emission at the tip from either field emission or Schottky enhanced photo-emission. Figure 2 provided by J. Lewellen shows the on axis field in a 1.5 cell rf gun with a needle cathode. The field enhancement at the tip of a 600 μm diameter needle with 200 μm flat-top radius is a factor of three above the field with a standard flat cathode. The benefit of a needle cathode is low emittance due to the small source size but the small source size also produces relatively low charge. The simulations predict an emittance of 0.1 μm with 20 pC of charge and a 4 ps flat-top pulse shape. The brightness from the needle is higher than a beam produced in a conventional photo-cathode since the emittance falls faster than the square root of charge. The thermal emittance from the needle cathode is assumed negligible due to the small source

size. M. Uesaka showed a Tungsten Needle photo-cathode experiment in a DC gun with a measured QE of 3%. There are plans to install the needle into an rf gun with calculations of over 100 A peak current with a 10 μm needle.

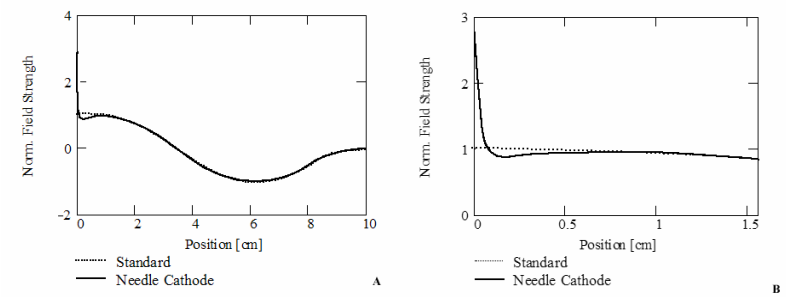

Figure 2. The on axis field versus position is plotted for both a needle and standard cathode. The axis has been expanded in (B) and it can be seen that the field at the needle tip is enhanced by a factor of three over a standard cathode. The plot was provided by J. Lewellen.

A fair amount of discussion was spent on cathodes but very few presentations were made on the subject. Most of the groups represented used metal cathodes but several groups utilize semiconductor cathodes. Metals still appear the most common choice often because of rf breakdown concerns, vacuum considerations and lifetime. M. Useaka reported a group in Japan is working on a metal transmission cathode where the laser is incident upstream of the cathode but no details were available. Nonetheless the group realized the work is interesting since it would allow for normal incidence laser operation without the need for a mirror installed near the electron beam creating undesirable wakefields. This can also be accomplished with grazing incidence laser operation. However, the laser optic corrections necessary to compensate for the elliptic beam and time dependent laser arrival time across the cathode often prevent groups from operating at grazing incidence.

3. Novel Injector Design

Pulsed DC electron guns [6] were one type of novel injector discussed. J. Luiten gave a plenary talk on the status of such guns. The pulsed DC guns described uses a photocathode inside a DC gun with GV/m fields for ns pulse durations to prevent breakdown. The electrons are accelerated over milimeter distances into the MeV energy range and exit through a hole in the anode. The pulsed DC gun allows higher gradients to be achieved in the gun and eliminates the time dependent rf focussing effects in conventional rf guns. It does not

completely eliminate the time dependent space charge term although the higher gradient helps reduce its effect. Simulations indicate the possibility of producing sub-micron emittance beams and several groups are now working on building and measuring the brightness from a pulsed DC gun. While these guns are likely many years from surpassing the rf photoinjector beam brightness currently achieved they are a promising and exciting new source.

A variant of the pulsed DC gun is a hybrid DC rf gun. A hybrid utilizes a pulsed DC gun feeding a standard rf photoinjector. The normal photocathode in the photoinjector is replaced by a plate with a small hole and the output of the pulsed DC gun is injected directly into the rf cavity. A. Zholents presented the hybrid design shown in Figure 3 which has been designed for kHz repetition frequencies. Standard room temperature photoinjectors are limited to 100 Hz or lower repetition rates due to cooling limitations from the high rf fields used for acceleration. However, with a pulsed DC gun at the front end, the rf fields can be substantially decreased eliminating the cooling problem and still accelerate the beam to a few MeV energy exiting the hybrid gun. Preliminary simulations indicate this can be accomplished with minimal effect on the beam brightness.

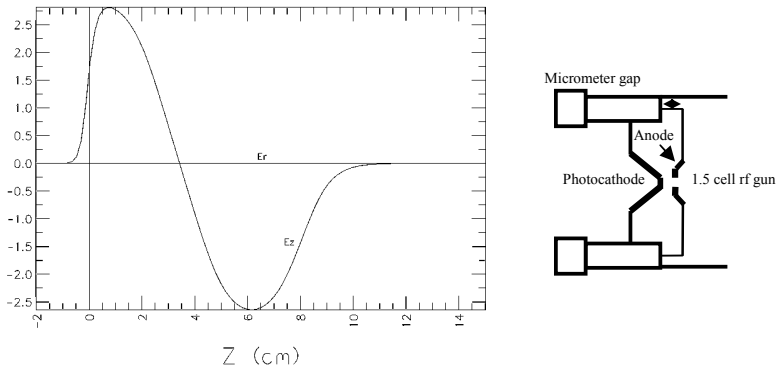

Figure 3. The on axis field as a function of longitudinal position for a Hybrid DC-rf gun is shown. A conceptual schematic for the photo-cathode and pulsed DC gun anode are also shown with an adjustable cathode position. The DC anode is immediately followed by a 1.5 cell S-band rf gun with a small hole in the standard cathode plate for electron injection from the pulsed DC gun. The figure was provided by A. Zholents.

As mentioned earlier S-band guns are not the only frequency of operation for rf photoinjectors. Lower frequency injectors have had success at producing high brightness beams such as ELSA 2 and the AFEL multicell rf gun [7]. These injectors suffer from undesireable effects such as limited gradient due to

rf breakdown, increased thermal emittance, long pulses often requiring additional bunch compression and subsequent problems associated with compression such as CSR. However, they are easy to fabricate, require relatively low solenoid field strengths and the laser pointing and timing jitter requirements are easier to meet due to the larger beam size.

Higher frequency rf guns have the ability to reach higher gradients, but generate lower charge per bunch, are more difficult to fabricate, require higher solenoid fields for emittance compensation and require more stringent requriements on the laser such as timing jitter and pointing stability. Several X-band rf guns have been fabricated and tested [8-9]. At even higher frequency in the optical regime are laser wake-field based injectors. These injectors were not discussed in the injector group but were included in working group D which covered laser acceleration schemes. From the discussion it was not clear at which rf frequency the beam brightness is maximized.

A flat beam photoinjector design was presented by S. Lidia. The salient differences in the described flat beam injector and a standard photoinjector is the imposition of a solenoid field at the cathode, and a skew quadrupole triplet immediately following the booster cavity. The large correlation in the 4D xy phase space of the beam as it leaves the solenoid field is translated into a large ratio between the x and y emittances with the removal of the cross correlation (xy', x'y) terms. Figure 4 shows a schematic of the beamline and some recent

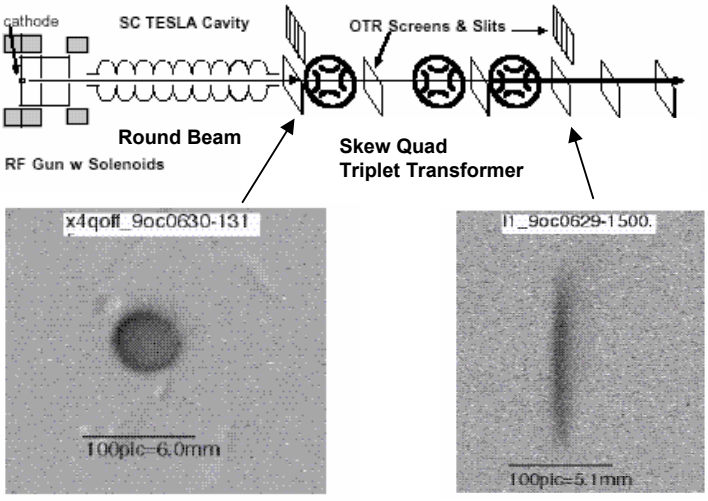

Figure 4. A schematic of the beamline for generating a flat beam is shown along with images of the electron beam before and after converting it to a flat beam with the skew quadrupole triplet. The figure was provided by S. Lidia.

experimental results of flat beam production at the A0 photoinjector facility at Fermilab. The source is intended for driving a recirculating linac with standard bending magnets and insertion devices to produce femto-second scale synchrotron radiation. The production of ultrafast radiation pulses involves a two-stage compression process. The first stage of compression compresses the electron beam from 20ps to 2ps and the second stage compresses the x-ray pulse from 2ps to 50-100fs in an asymmetric Bragg mirror pair. The last stage of compression requires a flat electron beam with low vertical emittance (<0.4 μm) and high horizontal emittance (~20 μm). Recent measurements with beams in the charge range of 200-300 pC and laser pulse lengths from 10-34 ps FWHM yield an emittance approximately 1-2 μm vertically and 30-50 μm horizontally.

4. Computational Modeling Issues

Several presentations were made on simulation codes. M. Quattromini talked about the code TREDI. TREDI is a fully 3D macroparticle Monte Carlo code devoted to the simulation of electron beams through rf guns, linacs, magnets and other beamline components where self fields are accounted for by means of Lienard-Wiechert retarded potentials. The code has been compared against PARMELA and HOMDYN using the SPARC project injector parameters. It was found to have good or excellent agreement with both codes when comparing beam sizes and energy spreads. The emittance predicted by the codes agree in the gun and solenoid region. However a discrepancy develops in the drift region where TREDI predicts the need for a slightly different solenoid position for optimal emittance. Additional work is underway to understand if this difference can be explained due to the use of Lienard-Wiechert potentials which are not used in the other codes.

C. Limborg presented a comparison between a slice emittance experiment at the Source Development Laboratory (SDL) at BNL and PARMELA simulation [10]. Comparison of all three Twiss parameters shows good agreement once careful measurements of all experimental parameters are input in the simulation including the thermal emittance, longitudinal and transverse profiles, solenoid map, and gun field map. It was discovered that decreasing the on axis gun field in the half cell by 20% from the design field was necessary to predict the beam sizes measured in the experiment. The study demonstrates that

simulations can match the experiment if all the experimental parameters are carefully measured. Figure 5 shows the simulated and measured slice Twiss parameters at the end of the SDL linac for two different solenoid current values.

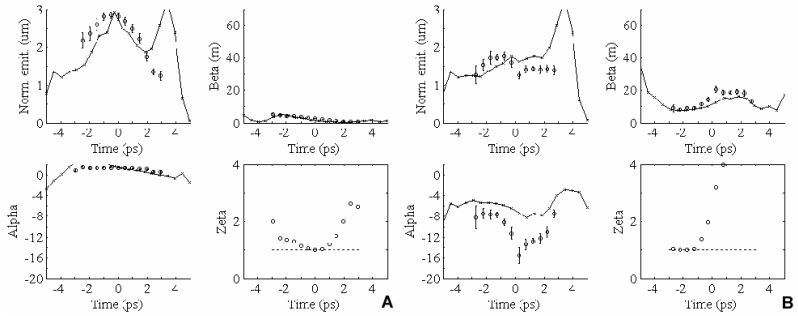

Figure 5. The simulated and measured Twiss parameters as a function of time are shown. The solenoid field is set at 98 A in (A) and 104 A in (B). Simulations are shown as solid lines and measured data as points. Zeta is commonly called the mismatch parameter. The figure was provided by C. Limborg.

C. Limborg also presented a PARMELA simulation of an emittance measurement experiment at the Gun Test Facility at SLAC. Typically, simulations report the emittance as the result of the calculation of the emittance from the full 6-D phase space distributions. However, typical experiments determine the emittance from measuring beam size only. In this experiment the rms beam sizes were determined by projecting a beam image in one plane and then truncating the wings at 5% of the peak value to minimize the effect in the data analysis of non-beam-related pixels. The Twiss parameters are then fit to the resulting rms beam sizes with the measured beamline parameters. In the simulation the beam sizes were computed identically but with different wing truncations values and the Twiss parameters fit to the results just like the experiment. Figure 6 shows a plot of the emittance as a function of the wing truncation level with 10,000 particles simulated in PARMELA and the particle number artificially increased during post processing to 100,000 particles to improve the statistics. As can be seen from the figure the total beam emittance is significantly underestimated with truncations greater than 2%. However, in real experiments the noise level is often above 2% and is the reason typical experiments use truncations as high as 10%. Thus, measured emittances can be less than the value computed by simulation. The study points out that care must be taken when comparing only the emittance value between simulation and experiment. A more accurate method is to compare all the Twiss parameters to be sure the simulation accurately describes the experiment since the emittance

parameter by itself can be misleading. The study also demonstrates the need for a large dynamic range in the electron beam imaging system to avoid truncation errors.

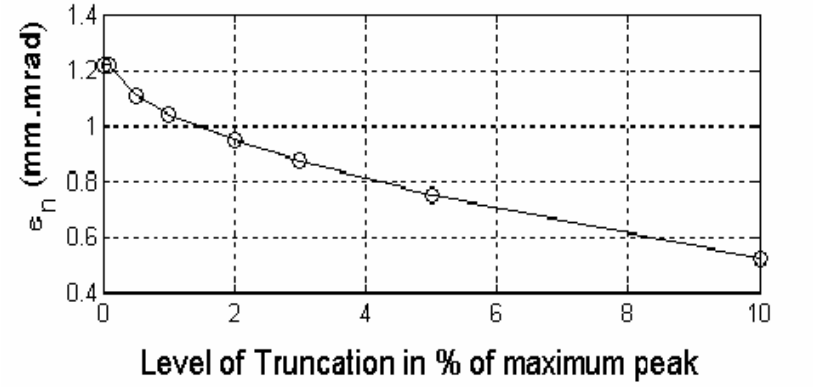

Figure 6. The computed emittance as a function of wing truncation level is shown for a typical set of beam parameters. The emittance computed by PARMELA from the full 6-D phase space distribution is 1.3 pm. The figure is provided by C. Limborg.

K. Floettmann pointed out that the phase space emittance is not constant in a drift under certain circumstances. The phase space beam emittance is the area of the ellipse in momentum-size space while trace space emittance is the area of the ellipse in divergence-size space. The two quantities are only exactly equal in a beam with no energy spread. With large energy spreads one finds that the emittance can vary significantly in a drift due to the development of the fan like or bow-tie phase space distributions. Figure 7 shows the phase space emittance and trace space emittance as a function of distance along the beamline. At various positions along the beam-line correlated energy spreads are added or removed and the effect on the two emittances can be observed. As can be seen in the figure the two emittances are not always identical and can be substantially different depending on where along the beamline they are computed. The study demonstrates that care is required when measuring the emittance of a beam with relatively large energy spread.

The discussion of simulation codes centered on additional effects that need to be included in simulations. Most of the codes used for photoinjectors do not include wakefields. Both transverse and longitudinal wakefields need to be included to explain some of the effects seen in measurements. Also, the

simulations do include the Shottky enhanced emission off the cathode. This mean that the time dependent emission off the cathode due to the changing rf and space charge field is not modeled and neither is the saturation effect as the charge nears the space charge limit. Finally, the simulations should be using measured values for thermal emittance and more accurate rise times for the drive laser. Despite the effects that are not included in the simulations, the agreement between experiment and simulations has substantially improved in recent years.

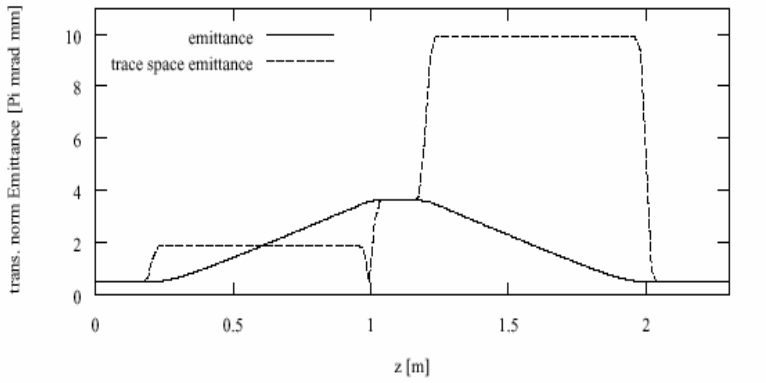

Figure 7. The normalized emittance and the normalized trace space emittance are plotted along a beamline. A beam with 5 mrad correlated beam divergence is launched at z = 0. A cavity at z = 0.2 m introduces a correlated energy spread of 2 10^{-3} which is compensated by another cavity at z = 1.0 m. A third cavity at z = 1.2 m introduces a correlated energy spread of -2 10^{-3} which is again compensated by a fourth cavity at z = 2.0 m. The figure was provided by K. Floettmann.

5. New Experimental Techniques and Results

With the large number of photoinjectors in operation world wide, it was no surprise that a large number of presentations concentrated on experimental results. Section 5.1 describes several of the experiments most relevant to high brightness beams. In addition a surprising amount of time was spent discussing data analysis techniques. The importance of proper data analysis for comparison with simulation values was pointed out by C. Limborg in the course of a study comparing experimental results with PARMELA simulations from several different photoinjectors. Errors associated with ignoring space charge in

the data analysis were also pointed out. Section 5.2 describes the data analysis issues and recommendations.

5.1. *Techniques and Results*

M. Uesaka presented results from Sumitomo Heavy Industries with emittance measurements as a function of laser pulse length and shape [1]. Nearly square or flat-top pulse shapes were generated using a spectral phase mask consisting of a liquid crystal modulator in the mid plane of a grating compressor. The pulse shapes were measured with a streak camera. Figure 8 shows both the laser pulse shape and the emittance measurements as a function of charge and laser pulse length for the Gaussian and square pulse shape. This is believed to be the first emittance measurement from a photoinjector with a square pulse shape drive laser. The emittance was measured to be 1.2 pm with 1 nC of charge with a 9 ps FWHM square laser pulse. The emittance is estimated to be a factor of two less

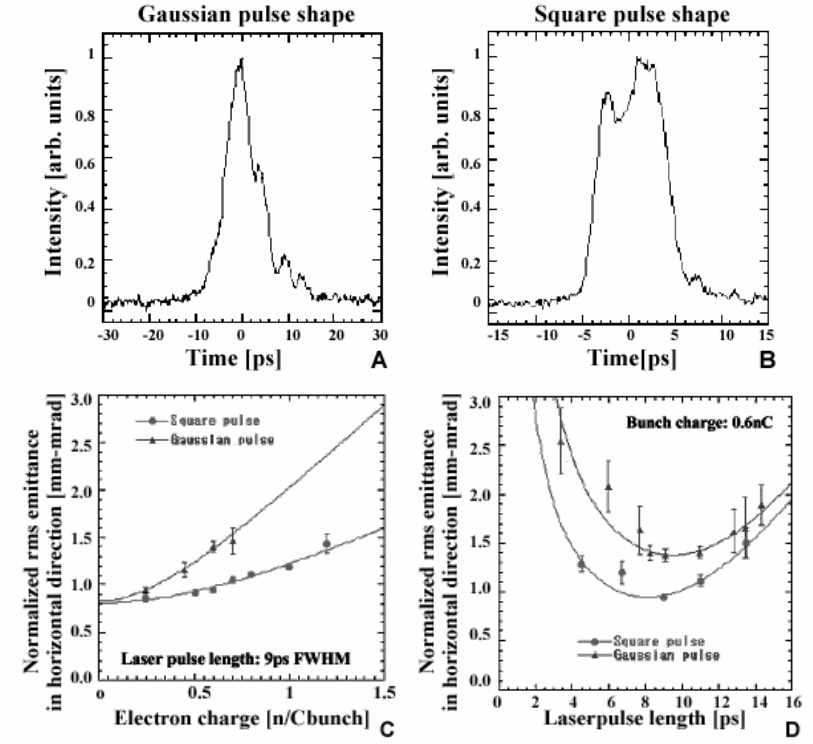

Figure 8. The measured laser pulse shape in (a) and (b) for the Gaussian and square pulse respectively with pulse length 10 ps FWHM. The emittance is plotted in (c) and (d) as a function of charge and laser pulse length respectively for both Gaussian and square pulse shapes. The figure was provided by J. Yang.

than the beam produced with an identical length Gaussian pulse. The thermal emittance can be extracted from the emittance as a function of charge curve and is estimated to be approximately 0.6 pm with an approximately 1 mm diameter Cu cathode.

J. Schmerge presented measured slice emittance results. Typical emittance measurements report only the projected emittance although simulations consistently show the emittance to be a function of longitudinal position. By introducing a time-energy correlation into the beam by appropriately setting the phase of the linac downstream of the gun, the emittance was measured as a function of time in a dispersive section using a quadrupole scan technique. The slice emittance measurements yield significantly more information than projected emittance alone since they reveal the presence of any longitudinal correlations and provide the means for removing them. Measurements were performed with 300 pc of charge with a 2 ps FWHM laser pulse as measured with a streak camera. The gun field was 110 MV/m with 30° extraction phase and the linac phase was set at +5° to appropriately chirp the beam exiting the linac at 30 MeV. Figure 9 shows the emittance as a function of slice for different values of the solenoid field. The projected emittance is plotted as slice 0 and the time axis is estimated at 200 fs/slice. The measurements show slice emittances as low as 2 pm with a Gaussian pulse shape and peak current of 150 A.

In addition to the transverse phase space measurements, a measurement of the longitudinal phase space was also performed. The longitudinal phase space was determined by measuring the energy spread at the exit of the linac as a function of linac phase. The technique is analogous to a quadrupole scan in transverse space. However, a quadratic and cubic term were added to the phase space ellipse description to account for the sinusoidal rf acceleration term and longitudinal space charge force respectively. The distribution at the linac entrance is mapped through the linac and is then fit to the measured energy spread exiting the linac. A large correlated energy spread is observed at the gun exit and is also shown in Figure 9. The energy spread is 8% FWHM and the longitudinal emittance is 4.6 keV ps.

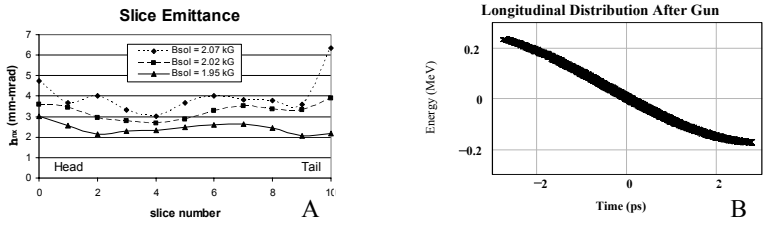

Figure 9. The emittance as a function of temporal slice is plotted for three different solenoid fields in (A). Slice 0 is the projection with slice 1 the head and slice 10 the tail of the beam. Each slice is approximately 200 fs long. The measured longitudinal distribution between the gun and linac is shown in (B). The beam has an approximately 8% correlated energy spread. The figure was provided by J. Schmerge and D. Dowell.

Additional longitudinal phase space measurements are under way at DESY Zeuthen on a 1.5 cell L-band gun with coaxial rf coupler. D. Lipka described the proposed experiment to use a Cherenkov radiator in a dispersive region with a streak camera to measure the longitudinal phase space. The experiment will allow the simultaneous measurement of energy spread, bunch length and correlations with better than 1 ps resolution. Figure 10 shows a schematic of the proposed experiment. Transverse emittance measurements directly exiting the gun are also planned using a pepper pot technique.

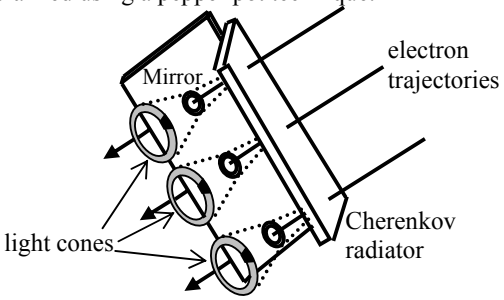

Figure 10. A schematic of the proposed Cherenkov radiator for measuring the longitudinal phase space. The light produced by the Cherenkov radiatior reflects of the mirror and is then incident into a streak camera. The figure was provided by D. Lipka.

Although the laser temporal and spatial profiles were identified as limiting factors in the achieved brightness from most existing rf photoinjectors, surprisingly little work was presented on improving the performance of the laser. H. Dewa did show a measured 33% decrease in the emittance by using a microlens array homogenizer to flatten the laser spatial profile. To date only one group has measured the emittance with a temporal flat-top laser pulse and

no measurement has yet been performed with both temporal and spatial flat-top profiles. D. Palmer presented timing jitter measurement on a Ti:sapphire laser oscillator. The measured rms jitter between the laser and rf source was less than 500 fs.

5.2. *Data Analysis*

One point of concern for the experimentalist in the group was data analysis. The algorithm used to convert beam images into spot sizes and the subsequent fitting routine can have a large impact on the measured emittance. The difference between rms and Gaussian fits to the beam spot size can be larger than 20% leading to almost 50% difference in the reported emittance from identical data. As shown in section 4 the amount of truncation when attempting an rms beam size measurement can lead to significant errors. Also, the beam size calculated from a single line out of an image versus a projection can be substantially different depending on the beam shape and orientation. The method used for emittance measurements such as quadrupole scan, pepper pot, two screen, multiple screen and single shot techniques all have various errors and different assumptions built into the analysis which can lead to discrepancies between measurements on identical beams. Finally, almost all of the emittance measurements reported in the literature assume that space charge is negligible over the length of the measurement. This is not always true and can have a large impact on the result. Thus comparing results between different machines and techniques is often misleading.

J. Rosenzweig demonstrated the effect of space charge on the emittance fit in a quadrupole scan. Typical quadrupole scans assume that the space charge term is small compared to the emittance term in the envelope equation. However, at relatively low energies, high charges or large beam sizes the space charge term can be significant and may have a large effect on the measured emittance. In a quadrupole scan and with no space charge, the square of the beam size is a parabolic function of the quadrupole focal length in the thin lens approximation. J. Rosenzweig showed that the beam size is also parabolic with focal length when the emittance term is neglected and only the space charge term is considered. The beam size as a function of focal length is no longer symmetric about the minimum spot size when both terms are significant. The asymmetric shape of the curve is a clear sign of the space charge effect. It should be pointed out that space charge actually dominates when the beam size is large since the space charge term is inversely proportional to the beam size and the emittance term is inversely proportional to the beam size cubed. Thus space charge actually dominates when the beam is large with all other

parameters being constant. Figure 11 shows the beam size as a function of quadrupole focal length with space charge only and with both the space charge and emittance terms included. As can be seen the curve with both terms is clearly asymmetric. However, despite the asymmetry the curve can still be fit without the space charge term although the fit will result in an error in the emittance.

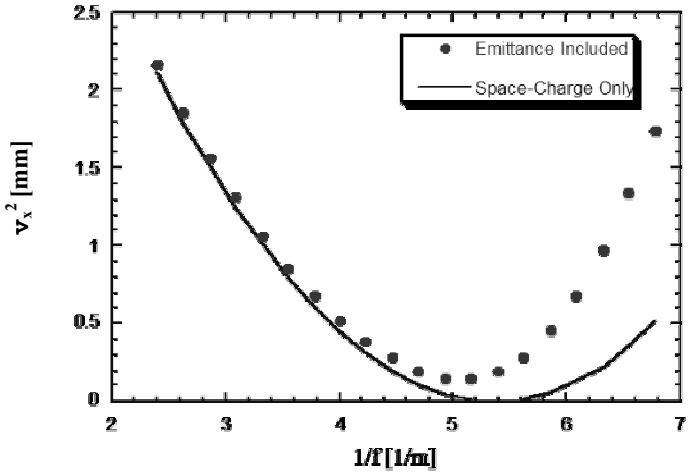

Figure 11. A plot of beam size versus quadrupole focal length is shown. The beam size is computed from the envelope equation. One curve uses only the space charge term and neglects the emittance term while the second curve includes both terms. The figure was provided by J. Rosenzweig.

In a typical quadrupole scan the emittance from a fit including space charge will be lower than the emittance obtained by neglecting space charge. This is due to the fact that the space charge force always acts to increase the beam size along the drift and the result is a larger beam at the screen than would be expected without space charge. In order to keep the beam size at the measured value when including space charge, the emittance used in the fit must be reduced. However, in multiple screen measurements with focusing elements between screens this is no longer necessarily true. Thus it is even more important to be sure space charge is negligible in multiple screen emittance measurements. Regardless of technique, space charge needs to be considered when analyzing emittance measurements.

The group agreed that in order to accurately compare results between groups and simulation, certain details of the measurement technique and

analysis need to be reported. The general consensus was that full projected images and rms spot sizes should be used since the envelope equation is derived for rms quantities. The truncation level used in the rms calculation of beam size should be as low as possible and also reported in the literature. Finally the effects of space charge should be included in the analysis.

Acknowledgments

The author would like to acknowledge all the participants in working group A for their valuable and timely presentations as well as the figures they provided that were used in this paper. The participants also posed numerous interesting questions, comments, and suggestions during the course of the workshop. In addition the author appreciated the lively debate during the discussion phase and the helpful suggestions in the summary preparation period. Although everyone assisted with the group summary, I would specifically like to acknowledge the assistance of J. Lewellen and C. Limborg for their aid preparing and editing the working group A summary. Finally I must acknowledge the help of A. Mueller with the graphics.

References

1. J. Yang, F. Sakai, T. Yanagida, M. Yorozu, Y. Okada, K. Takasago, A. Endo, A. Yada and M. Washio, *Jrn. App. Phys. Rev.* **92**, 1608 (2002).
2. J.-G. Marmouget, A. Binet, Ph. Guimbal and J.-L. Coacolo, "Present performance of the low-emittance, high-bunch charge ELSA photo-injected linac" *Submitted to EPAC 2002*, Paris, June (2002).
3. See the LCLS home page at http://www-ssrl.slac.stanford.edu/lcls/
4. G.R. Neil, *Nucl. Instr. Meth. A* **483**, 14 (2002).
5. W.S. Graves, L.F. DiMauro, R. Heese, E.D. Johnson, J. Rose, J. Rudati, T. Shaftan and B. Sheehy, *Proceed. PAC 2001* 2227 (2001).
6. K. Batchelor, J.P. Farrell, G. Dudnikova, I.Ben-Zvi, T. Srinivasan-Rao, J. Smedley and V. Yakimenko, *Proceed. EPAC 1998* 791 (1998).
7. S.M. Gierman, in *The Physics of High Brightness Beam*s, World Scientific, 511 (2000).
8. W.J. Brown, K.E. Kreischer, M.A. Shapiro, R.L. Temkin and X. Wan, in *The Physics of High Brightness Beam*s, World Scientific, 454 (2000).
9. A.E. Vlieks, G. Caryotakis, R. Loewen, D. Martin, A. Menegat, E. Landahl, C. DeStefano, B. Pelletier, N.C. Luhmann, Jr., *SLAC-PUB-9354,* (2002).
10. W.Graves et al. "Experimental study of sub-ps slice electron beam parameters in a photoinjector" *Submitted to Phys. Rev. ST-AB*, (2002).